

Redundant and Nonredundant Information for Model Calibration or Hydraulic Tomography

by Jet-Chau Wen^{1,2}, Jyun-Lin Chen³, Tian-Chyi Jim Yeh⁴, Yu-Li Wang⁴, Shao-Yang Huang⁵, Zhong Tian⁶, and Chia-Yii Yu⁷

Abstract

Drawdown data from independent pumping tests have widely been used to validate the estimated hydraulic parameters from inverse modeling or hydraulic tomography (HT). Yet, the independent pumping test has not been clearly defined. Therefore, the goal of this paper is to define this independent pumping test concept, based on the redundant or nonredundant information about aquifer heterogeneity embedded in the observed heads during cross-hole pumping tests. The definition of complete, moderate redundancy and high nonredundancy of information are stipulated using cross-correlation analysis of the relationship between the head and heterogeneity. Afterward, data from numerical experiments and field sequential pumping test campaigns reinforce the concept and the definition.

Introduction

Characterization of aquifer hydraulic properties is essential for groundwater resources management, as well as groundwater contamination prevention and remediation. Aquifers are inherently heterogeneous

at a multiplicity of scales. Traditional aquifer analyses, such as the Theis solution (Theis 1935) and Cooper-Jacob approximation (Cooper Jr and Jacob 1946), nevertheless, adopts aquifer homogeneity assumption for the sake of parsimony even though they are comparing apples and oranges as criticized by Wu et al. (2005). In addition, Wu et al. (2005), Wen et al. (2010), Huang et al. (2011), and Yeh et al. (2015) found that the estimates from the traditional analyses are scenario-dependent—the estimates vary from one test to another test. This scenario-dependency was also reported by Huang et al. (2011) and Yeh et al. (2015) in the estimated parameter fields derived from calibrating highly parameterized conceptual models.

Over past decades, a new generation of aquifer test technology, hydraulic tomography (HT), has been developed to overcome the difficulties associated with the traditional aquifer tests and to map heterogeneous hydraulic properties of aquifers (e.g., Yeh and Liu 2000; Liu et al. 2002; Brauchler et al. 2003; Li et al. 2005; Zhu and Yeh 2005, 2006; Illman et al. 2007, 2008, 2010, 2012, 2015; Liu et al. 2007; Fienen et al. 2008; Hao et al. 2008; Ni and Yeh 2008; Castagna and Bellin 2009; Ni et al. 2009; Xiang et al. 2009; Yin and Illman 2009; Cardiff and Barrash 2011; Liu and Kitanidis 2011; Mao et al. 2011, 2013c; Berg and Illman 2011a; Sun et al. 2013; Zhao et al. 2015; Tso et al. 2016). After decade's applications, HT has been accepted as a mature and viable technology for mapping aquifer heterogeneity distributions. HT can obtain hydraulic property estimates that can yield better predictions of flow and solute transport in aquifers than those by traditional approaches (Illman et al. 2008, 2009, 2010, 2012) and Ni et al. (2009).

¹Department of Safety, Health and Environmental Engineering, National Yunlin University of Science and Technology, 123, Section 3, University Road, Douliou 64002, Yunlin, Taiwan.

²Research Center for Soil and Water Resources and Natural Disaster Prevention, National Yunlin University of Science and Technology, 123, Section 3, University Road, Douliou 64002, Yunlin, Taiwan.

³Doctoral Program, Graduate School of Engineering Science and Technology, National Yunlin University of Science and Technology, 123, Section 3, University Road, Douliou 64002, Yunlin, Taiwan.

⁴Department of Hydrology and Atmospheric Sciences, University of Arizona, John Harshbarger Building, 1133 E. North Campus Drive, Tucson, AZ 85721, USA.

⁵Corresponding author: Research Center for Soil and Water Resources and Natural Disaster Prevention, National Yunlin University of Science and Technology, 123, Section 3, University Road, Douliou 64002, Yunlin, Taiwan; 886-937-020761; syh1019@ntu.edu.tw

⁶State Key Laboratory of Hydraulics and Mountain River Engineering, Sichuan University, 24, South Section 1, Yihuan Road, Chengdu 610065, China.

⁷Safety, Health, and Environmental Center, Group Administration, Formosa Plastics Group, 201, Tunghwa North Road, Taipei 10508, Taiwan.

Article impact statement: The concept of complete, moderate redundancy, and high nonredundancy of head data sets can be validated by hydraulic tomography.

Received March 2018, accepted March 2019.

© 2019, National Ground Water Association.

doi: 10.1111/gwat.12879

Despite this evidence, Bohling and Butler (2010) argued that the drawdown data of the sequential pumping test (or HT) are not necessarily independent records (i.e., redundant information) according to the reciprocity principle (Bruggeman 1972). The reciprocity principle states that the drawdown-time behavior at location A caused by pumping at location B is the same as that at location A due to pumping at location B. In other words, the head observed at Well A due to pumping at Well B is affected by the same heterogeneity as is the head observed at Well B induced by pumping at Well A. Specifically, the heads collected from the two pumping tests carry redundant information about the aquifer heterogeneity.

Redundant/nonredundant head data sets play critical roles on the inverse modeling efforts as well. For instance, Huang et al. (2011) (Figure 5) reported that using 11 wells and sequentially increasing the number of pumping events in a synthetic aquifer, the estimated transmissivity (T) field continuously changed, improved, and stabilized at a T field, which closely resembles the reference field. That is, the head data sets from 10 observation wells induced by one pumping test cannot conclusively define the heterogeneity of an aquifer unless data sets from additional pumping tests are included. Consequently, collecting head data sets, which carry new information about the heterogeneity, becomes an important issue in model calibration practices. This importance was also advocated in Mao et al. (2013a, 2013b, 2013c), which reported the nonredundant information can improve the estimates about the heterogeneity in variably saturated zones.

Similarly, nonredundant head information is critical for validating estimated parameters from inverse modeling efforts. For example, Illman et al. (2007, 2008) and Liu et al. (2007) validated the estimated parameter fields from HT using independent pumping test data in sandbox experiments. Berg and Illman (2011b) carried out validation of HT in the field aquifer. Huang et al. (2011) also utilized additional pumping tests to verify the estimates from HT of a field aquifer. Likewise, using independent pumping tests data, Zhao et al. (2016) and Zhao and Illman (2017, 2018) evaluated hydraulic property estimates from HT analyses with the prior geologic information. Independent pumping test data sets were employed by Zha et al. (2015, 2016) to confirm HT estimates for fractured granite rock mass.

The independent pumping tests reported in the previous studies generally were conducted at the wells which were used as the head observation wells in their HT calibration. Because of this fact, the heterogeneity information contained in the heads induced by the independent pumping tests at these wells likely have been explored by the earlier HT analysis. The validation, therefore, may not be conclusive. For this reason, there is a need to define the independent pumping test or to clarify the redundant and nonredundant information about aquifer heterogeneity embedded in observed head data sets. In

order to investigate these issues, this paper first uses cross-correlation analysis to define completely, moderately redundancy and highly nonredundancy of head data. Then, it uses datasets from 11 pumping tests with 11 wells in the heterogeneous synthetic and field aquifers to derive the best-estimated fields using the HT analysis. Afterward, the best-estimated T and storage coefficient (S) fields are then validated to corroborate the definition of redundancy and nonredundancy.

Completely, Moderately Redundant, and Highly Nonredundant Information

Cross-Correlation Analysis

A quantitative means to define completely, moderately redundant, or highly nonredundant information about heterogeneity embedded in the head observation is the cross-correlation between the observed head and heterogeneity in every part of an aquifer. According to Sun et al. (2013) and Wu et al. (2005), in order to analyze the relationship between the head and $\ln T$ and that between the head and $\ln S$ values in a heterogeneous aquifer, $\ln T$ and $\ln S$ at every location of the aquifer can be treated as random variables with some spatial correlation with others in the adjacent locations. Specifically, $\ln T = Y + y$ and $\ln S = Z + z$, where Y and Z are mean values, and y and z denote perturbations, which represent spatial variability or uncertainty due to lack of measurements of these parameters. For the same reason, the head is represented by $H = \bar{H} + h$, where \bar{H} is the mean and h is the perturbation caused by spatial variability or uncertainty of the parameters. Using the first-order approximation, the head perturbation at the location \mathbf{x}_i at a given time t is then given as

$$h(\mathbf{x}_i, t) \approx \left[\frac{\partial H(\mathbf{x}_i, t)}{\partial \ln T(\mathbf{x}_j)} \Big|_{Y,Z} \right] y(\mathbf{x}_j) + \left[\frac{\partial H(\mathbf{x}_i, t)}{\partial \ln S(\mathbf{x}_j)} \Big|_{Y,Z} \right] z(\mathbf{x}_j)$$

$$\mathbf{h} = \mathbf{J}_{hy}\mathbf{y} + \mathbf{J}_{hz}\mathbf{z} \quad (1)$$

where $y(\mathbf{x}_j)$ and $z(\mathbf{x}_j)$ are perturbation of $\ln T$ and $\ln S$ at location \mathbf{x}_j and $j = 1, \dots, N$, which is the total number of parameters in the aquifer (i.e., number of elements in a finite element domain); $J_{hy}(\mathbf{x}_j, \mathbf{x}_j, t)$ and $J_{hz}(\mathbf{x}_j, \mathbf{x}_j, t)$ are the sensitivity of h at location \mathbf{x}_i at a given time t with respect to $\ln T$ and $\ln S$ perturbation at location \mathbf{x}_j . Here, the Einstein's summation convention over the repeated suffix is used. That is to say, the head perturbation at (\mathbf{x}_i, t) is a weighted sum of perturbation of parameters $\ln T$ and $\ln S$ everywhere in the aquifer. The weights are the corresponding sensitivity values. Since the perturbations of the parameters are unknown, it is best to adopt the aforementioned stochastic representation of these parameters. Using the assumption that $\ln T$ and $\ln S$ are mutually independent of each other, the cross-covariance matrices between h and y and between h and

z are.

$$\begin{aligned} R_{hy}(\mathbf{x}_i, \mathbf{x}_j, t) &= J_{hy}(\mathbf{x}_i, \mathbf{x}_j, t) R_{yy}(\mathbf{x}_i, \mathbf{x}_j) \\ R_{hz}(\mathbf{x}_i, \mathbf{x}_j, t) &= J_{hz}(\mathbf{x}_i, \mathbf{x}_j, t) R_{zz}(\mathbf{x}_i, \mathbf{x}_j) \end{aligned} \quad i, j = 1, \dots, N \quad (2)$$

$R_{yy}(\mathbf{x}_i, \mathbf{x}_j)$ and $R_{zz}(\mathbf{x}_i, \mathbf{x}_j)$ are covariance matrices of perturbation of $\ln T$ and $\ln S$, which are modeled with the same exponential function using the same correlation scales in x and y directions. The corresponding head covariance matrix based on Equation 1 is given as

$$\begin{aligned} R_{hh}(\mathbf{x}_i, \mathbf{x}_j, t) &= J_{hy}(\mathbf{x}_i, \mathbf{x}_j, t) R_{yy}(\mathbf{x}_i, \mathbf{x}_j) J_{hy}(\mathbf{x}_i, \mathbf{x}_j, t) \\ &+ J_{hz}(\mathbf{x}_i, \mathbf{x}_j, t) R_{zz}(\mathbf{x}_i, \mathbf{x}_j) J_{hz}(\mathbf{x}_i, \mathbf{x}_j, t) \end{aligned} \quad (3)$$

The components of $R_{hh}(\mathbf{x}_i, \mathbf{x}_j, t)$ at $\mathbf{x}_i = \mathbf{x}_j$ are the head variances, $\sigma_{hh}^2(\mathbf{x}_i, t)$, which represents the uncertainty in the head at the location \mathbf{x}_i at a given time t due to the unknown heterogeneity in the aquifer. The cross-covariances, R_{hy} and R_{hz} , are then normalized by the square root of the product of the variances of h at (\mathbf{x}_i, t) and $\ln T$ or those of h at (\mathbf{x}_i, t) and $\ln S$ to obtain their corresponding cross-correlation ρ_{hy} , ρ_{hz} at location i and j at time t .

$$\begin{aligned} \rho_{hy}(\mathbf{x}_i, \mathbf{x}_j, t) &= \frac{J_{hy}(\mathbf{x}_i, \mathbf{x}_j, t) R_{yy}(\mathbf{x}_i, \mathbf{x}_j)}{\sqrt{\sigma_h^2(\mathbf{x}_i, t) \sigma_y^2}} \\ &= \frac{J_{hy}(\mathbf{x}_i, \mathbf{x}_j, t) R_{yy}(\mathbf{x}_i, \mathbf{x}_j)}{\sqrt{R_{hh}(\mathbf{x}_i, \mathbf{x}_i, t) R_{yy}(\mathbf{x}_j, \mathbf{x}_j)}} \\ \rho_{hz}(\mathbf{x}_i, \mathbf{x}_j, t) &= \frac{J_{hz}(\mathbf{x}_i, \mathbf{x}_j, t) R_{zz}(\mathbf{x}_i, \mathbf{x}_j)}{\sqrt{\sigma_h^2(\mathbf{x}_i, t) \sigma_z^2}} \\ &= \frac{J_{hy}(\mathbf{x}_i, \mathbf{x}_j, t) R_{zz}(\mathbf{x}_i, \mathbf{x}_j)}{\sqrt{R_{hh}(\mathbf{x}_i, \mathbf{x}_i, t) R_{zz}(\mathbf{x}_j, \mathbf{x}_j)}} \end{aligned} \quad (4)$$

where $\sigma_h^2(\mathbf{x}_i, t)$ is the head variance at \mathbf{x}_i and t ; σ_y^2 and σ_z^2 are the variances of $\ln T$ and $\ln S$, respectively. The cross-correlation (dimensionless) represents how the head perturbation at the location \mathbf{x}_i at a given time t is influenced by the $\ln T$ or $\ln S$ perturbation at a location \mathbf{x}_j in an ensemble sense. With a given mean T , S and a pumping rate, these cross-covariances are evaluated numerically using the HT inverse model by Zhu and Yeh (2005).

To elucidate the completely, moderately redundant and highly nonredundant information using the cross-correlation, Equation 4 was evaluated using numerical simulations. For this simulation, a square-shaped synthetic two-dimensional confined aquifer (200 m \times 200 m) was discretized into 100 \times 100 square elements with 2 m in length and width. The initial and boundary conditions were 100 m. A constant discharge of 0.0006 m³/s was imposed at a pumping well and heads were collected at an observation well. These two wells were separated by a distance of 40 m (see Figure 1). The geometric mean

values of T and S of the aquifer were 0.000116 m²/s and 0.00014, respectively. The variance of $\ln T$ was 1.0 and the variance of $\ln S$ is 0.2. Covariance functions of T and S were assumed to be the exponential model with isotropic correlation scales in x and y directions equal to 30 m. These input parameters were those used by Sun et al. (2013). Cross-correlation analyses of four cross-hole pumping tests were conducted using the synthetic aquifer.

The cross-correlation distribution at a late time pumping test is illustrated in Figure 1a. As shown in the figure, the cross-correlation coefficient (ρ_{hy}) between the head at the observation well and $\ln T$ everywhere forms two symmetrical kidney-shaped humps (where cross-correlation values greater than 0.4) near the observation well (the white circle in the figure) and the pumping well (the black circle). This means that the observed head is dictated by the heterogeneity within these two humps.

If the locations of the pumping well and the observation well are exchanged (test 2, Figure 1b), the two humps cover the same areas of the aquifer as those in Figure 1a. That is, the observed heads in these two figures are always dominated by the same variation of T in the aquifer; the observed heads thus contain the same heterogeneity information. Specifically, the heads at the observation well in tests 1 and 2 carry completely redundant (i.e., the same) information about the heterogeneity. This corroborates the reciprocity principle.

In Figure 1c (test 3), the ρ_{hy} is plotted for the case where the pumping well (the black circle in the figure) locates at the same location as that in Figure 1a but the observation well (the white circle) is moved to a new location. To avoid boundary effects due to small domain size, this relocation of the two wells was accomplished by rotating the two wells by 45° from the horizon with the pivot at the location ($x = 100, y = 100$). The shape of the two kidney-shaped humps (where cross-correlation values greater than 0.4) in Figure 1c remains the same as those in Figure 1a and 1b. After moving the observation well, the hump near the pumping well covers similar areas of the aquifer as those in Figure 1a and 1b. To the contrary, the hump near the observation well encompasses a different portion of the aquifer. Thus, the observed head will be dominated by the heterogeneity in this new location while retains the influence of the heterogeneity in the hump near the pumping well. This information content of the observed head is, thus, called the moderately nonredundant information.

As illustrated in Figure 1d, once the locations of the pumping and the observation well (i.e., the black and the white circle, respectively in the figure) are moved to completely different locations from those in Figure 1a and 1b, the two humps cover two different parts of the aquifer accordingly. Since the head at the observation well is dictated by the heterogeneity in the two humps, the heterogeneity information ingrained in the observed head will be highly different from those in Figure 1a and 1b. As a consequence, the head data from this new pumping and observation locations are referred to as

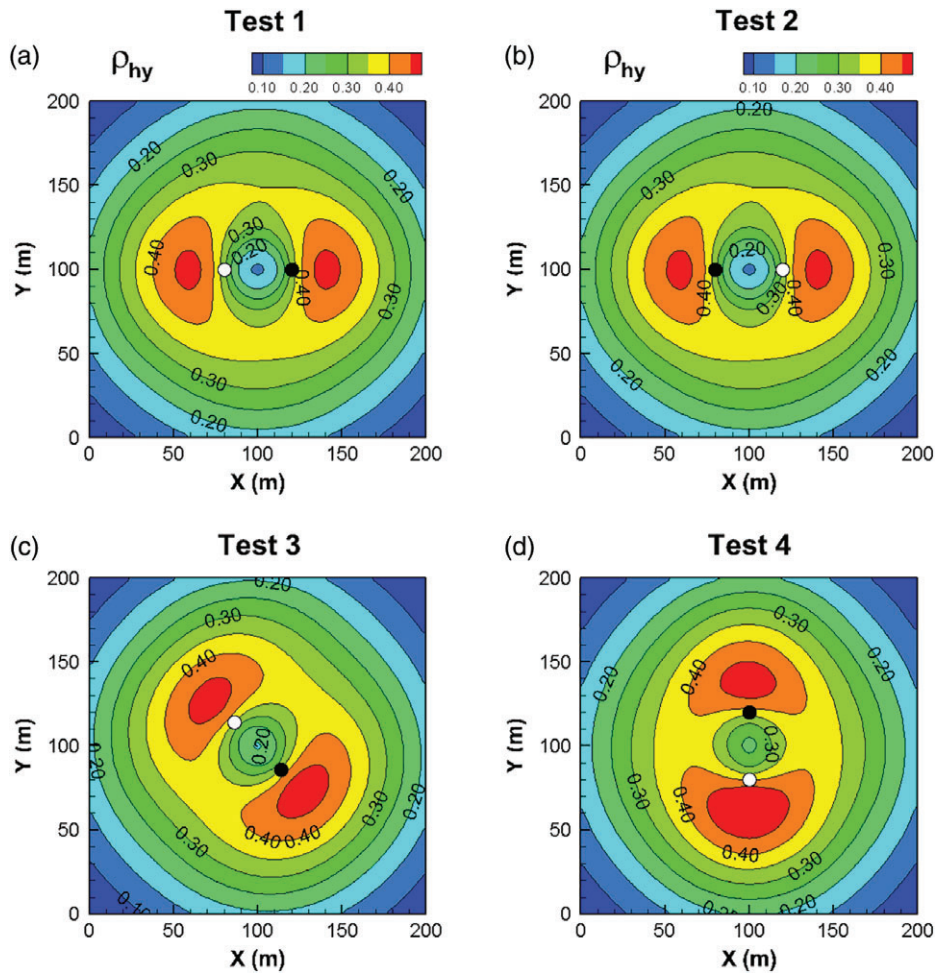


Figure 1. Contour maps of cross-correlation coefficient between the head at the observation well and $\ln T'$ everywhere in the aquifer while the flow reached steady-state. The white circle represents the location of observation well, and the black circle represents the location of the pumping well. (a) Test 1, (b) Test 2, (c) Test 3, (d) Test 4.

highly nonredundant information in comparison with the head data from the well setup in Figure 1a and 1b.

We emphasize the fact that any head (except at the constant head boundaries) in an aquifer is correlated with (or sensitive to) hydraulic conductivity at every part of the aquifer but with different degrees. For this reason, the above definitions are solely built upon the high correlation areas (i.e., the contour level of 0.4 and above) in the cross-correlation maps of two pairs of pumping and observation locations. Since the head in the observation is always influenced by heterogeneity in every part of the aquifer, the term, highly nonredundancy, is most appropriate to avoid confusion.

Furthermore, it is necessary to stress the fact that the cross-correlation analysis rests upon the ensemble statistics concept since the heterogeneity is not known. Specifically, the head perturbation in Equation 1 depends on the magnitudes of its sensitivity to every parameter in the aquifer as well as the magnitude of the parameter perturbation. However, the true parameter field is unknown such that the sensitivity has to be evaluated at the mean value of the parameter field. By the same token, the parameter perturbation is undetermined, and

the cross-correlation analysis thus relies on the variance of the parameters and in turn, the head variance, rather than their perturbations. That is to say, the uncertainties of the parameters (all possible parameter perturbation around its mean in a statistical sense) at the locations with the same cross-correlation values contribute equally to the uncertainty of the head at the observation well (i.e., all possible head perturbations in a statistical sense at this observation well). The actual contribution to the head perturbation at the observation well depends on the actual parameter perturbation at these locations, rather than the variance of the parameters. That is, in one realization of the heterogeneous aquifer, the contribution to the observed head perturbation from a location depends on not only the cross-correlation but also the parameter perturbation. Note that the reciprocity principle holds for one single realization since the two kidney shapes of high cross-correlations are symmetrical around the observation and pumping wells. Due to this symmetry, different parameter perturbations in each kidney area still contribute equally to the observed head regardless of the pumping and the observation well locations.

With the ensemble nature of the cross-correlation analysis in mind, the following numerical and field experiments are conducted to test and verify the above definitions of completely redundant, moderately redundant, and highly nonredundant information.

Pumping Test Experiments at the Field Site

The numerical experiment and field experiments are built on the sequential pumping test experiments conducted at a field site on the north side of the National Yunlin University of Science and Technology (NYUST) campus in Taiwan. Detailed information for the field site (geological information, wells, setting conditions, etc.) can be found in Wen et al. (2010), Huang et al. (2011), and Chen et al. (2019). The aquifer was considered a confined aquifer, according to Wen et al. (2010). In this site, 17 fully penetrating wells were installed over an area of 144 m². These wells were divided into two categories; 11 wells in 0.1016 m (4") diameter, and 6 wells in 0.0508 m (2") diameter, respectively. A detailed setup can be found in Figure 2. These wells were named as BH01, BH02 through BH11, and BH12 through BH17, respectively. Previous studies (Wen et al. 2010; Huang et al. 2011; Chen et al. 2019) used the data sets obtained from the 11 wells in 4" diameter but the 6 wells in 2" diameter. This was due to these wells in 2" diameter were primarily used for water quality monitoring. After 2010, these wells were used as observation wells in sequential pumping tests.

A total of 11 pumping tests were conducted in sequential order. A submersible pumping system (Grundfos Pumps Corporation), including the MP1 type of the water pump and variable-frequency drive, was utilized for the pumping tests in 2010 (Chen et al. 2019). Pressure transducers with a data logger (precision of 1 mm) were installed in all the 17 wells in order to collect the drawdown data. All pumping tests were conducted when there was no precipitation. In each pumping test, one of the 11 wells was pumped, and the heads were collected at the remaining 16 wells (Figure 2). Each pumping test lasted for 72 h to reach a steady flow condition. A new pumping test at another well began only after the groundwater level was fully recovered from the last test. Overall, 11 pumping tests were carried out, yielding 11 sets of drawdown data that included 176 drawdown-time curves (110 sets of 11 wells in 4" diameter, and 66 sets of 6 wells in 2" diameter—the pumping wells were excluded as previously mentioned). The pumping tests conducted in 2010 lasted from August 2010 to February 2011. The pumping rates of the 11 tests varied from 9.42 to 12.96 m³/d (Table 1) while a constant pumping rate was maintained for each test.

Pumping Tests in the Synthetic Aquifer

In order to create drawdown-time data sets for the synthetic aquifer mimicking the field experiments, a simulation domain (30 m × 30 m, Figure 2) was selected in such a way such that it includes all the 17 wells of

the field site. The domain was then discretized into 900 elements of 1 m × 1 m. All the 17 wells were distributed within the red square zone, which has 441 elements as shown in Figure 2. The boundary and initial conditions were the arithmetic average of the observed static water level (46.44 m) of the 11 wells in 4" diameter of the field champing.

The distribution of T and S values of the synthetic aquifer were generated using the spectral method (Gutjahr 1989; Robin et al. 1993) with the following spatial statistics: The $\ln T$ (natural logarithm of T) field had a mean of 2.430, and a variance of 1.0; The $\ln S$ (natural logarithm of S) field had a mean of -5.075 , a variance of 0.599; the spatial structure was described by an isotropic exponential covariance function with a correlation scale of 5 m in both directions. These spatial statistics were derived from Huang et al. (2011). The generated reference field of T and S are shown in Figures 4c and 5c. Afterward, the forward simulation was conducted using the VSAFT2 (variably saturated flow and solute transport in 2D, available at <http://tian.hwr.arizona.edu/downloads>) (Yeh et al. 1993). The pumping rates were the same as those of the field experiments.

From both the field experiment and the simulated experiment in the synthetic aquifer, 176 drawdown data (110 sets of 11 wells in 4" diameter, and 66 sets of 6 wells in 2" diameter) were collected from the 11 pumping tests. A total of 110 observed drawdown-time curves were selected for estimating the T and S fields. The remaining 66 drawdown data were used for validation modeling (i.e., to test the ability of the estimated T and S field for predicting the head fields under different pumping tests).

Best-Estimated T and S Fields

For testing and verifying the definitions of redundancy of the head information, the head data sets from the field experiments and numerical experiments from the synthetic aquifer were utilized to estimate the T and S of the corresponding aquifers. The estimation was carried out using HT analysis included in VSAFT2; the HT analysis uses the SimSLE inverse algorithm, which has described in numerous publications. Please refer to the work by Xiang et al. (2009) for details.

Selection of drawdown-time data from a well hydrograph for the HT analysis adopted the sampling strategy suggested by Sun et al. (2013). That is, since the drawdown is most sensitive to change in S at the early time of the drawdown-log time curve, three data points at small time intervals were selected at an early time, and the other four points were distributed over the rest of drawdown-time curve (i.e., seven drawdown values at different times). Details of the sampling method can be found in Chen et al. (2019). Figure 3 shows that the pressure heads were selected based on different time periods for each drawdown curve.

The mean absolute error (L1 norm), mean square error (L2 norm), and linear regression analysis with a standard correlation coefficient (COR, r) ($0 \leq |r| \leq 1$)

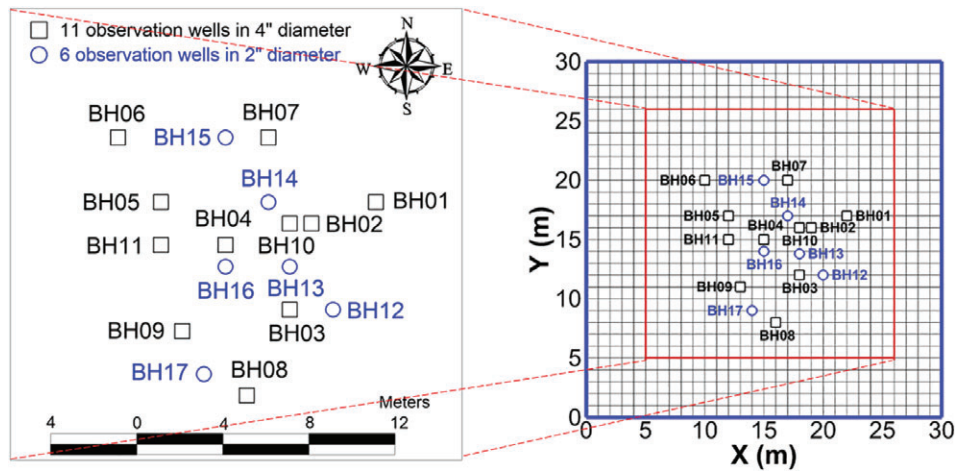


Figure 2. Well locations on NYUST campus site; two-dimensional hydrogeological numerical modeling. Each grid is 1 m x 1 m, the total model domain is 30 m x 30 m, and the boundary conditions (blue lines) are the prescribed head. The area indicated by the red square is 21 m x 21 m (441 grids) is the focus of the discussion in this paper.

Table 1
Control Conditions of the Sequential Pumping Tests (Year 2010)

Pumping Well Number	Pumping Rates Q (m ³ /d)	Observation Wells	
		4" Diameter	2" Diameter
BH01	11.84	BH02, 03, 04, 05, 06, 07, 08, 09, 10, 11	BH12, 13, 14, 15, 16, 17
BH02	12.42	BH01, 03, 04, 05, 06, 07, 08, 09, 10, 11	
BH03	11.76	BH01, 02, 04, 05, 06, 07, 08, 09, 10, 11	
BH04	12.86	BH01, 02, 03, 05, 06, 07, 08, 09, 10, 11	
BH05	12.83	BH01, 02, 03, 04, 06, 07, 08, 09, 10, 11	
BH06	12.74	BH01, 02, 03, 04, 05, 07, 08, 09, 10, 11	
BH07	12.96	BH01, 02, 03, 04, 05, 06, 08, 09, 10, 11	
BH08	12.68	BH01, 02, 03, 04, 05, 06, 07, 09, 10, 11	
BH09	12.81	BH01, 02, 03, 04, 05, 06, 07, 08, 10, 11	
BH10	9.42	BH01, 02, 03, 04, 05, 06, 07, 08, 09, 11	
BH11	10.68	BH01, 02, 03, 04, 05, 06, 07, 08, 09, 10	

were used as the performance criteria for the analysis in this study.

Synthetic Aquifer

Before analyzing the field experimental data sets, we determined the minimum number of pumping tests required to obtain the best-estimated fields in the synthetic aquifer first. For this purpose, we first randomly selected two tests (each test involves pumping at one well and observed drawdowns at another well to obtain drawdown-time data, and we have two drawn-time data sets), and we named the two drawdown-time data sets as D#2. Afterward, we added another well, chosen arbitrarily. Now, we have three wells; while pumping at each well, we observe drawdowns at the other two wells, and thus the number of the datasets increases to 6. This data set is then called D#3. In the case of D#4, we have four wells, we pump each one of the four wells and monitor the drawdown at the other three wells, and we have a total of 12 drawdown-time data sets. This addition

of pumping tests, as well as the nomenclature of the data sets, was continued until the total number of pumping tests reached 11, and the total number data sets became 110, which is the final data set, called D#11. Table 2 lists the wells and the number of drawdown-time curves associated with each dataset.

Subsequently, inverse modeling exercises using each data set were carried out. The scatter plots and evaluation criteria for the estimated $\ln T$ and $\ln S$ fields were calculated with respect to the reference T and S fields. While the data sets were used to estimate T and S of 900 elements but only those around the wells (441 elements) were evaluated for the best-estimated field.

The scatter plots of the best-estimated $\ln T$ and $\ln S$ fields vs. those of the reference field as well as associated L1, L2, and COR are shown in Figures 4a and 5a, respectively. These figures show that the estimated and reference $\ln T$ and $\ln S$ values were distributed along the 45° line, indicative of unbiased estimates but with some degree of scattering. The COR of $\ln T$ and $\ln S$ fields were

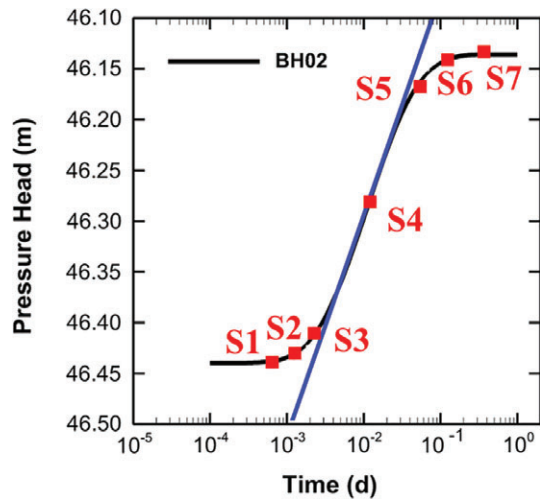


Figure 3. Concept plot of the sampling method.

0.832 and 0.811, respectively. The best-estimated T fields are illustrated in Figure 4b; the S fields are displayed in Figure 5b. These best-estimated fields were the result of using dataset D#9. Using D#10 and D#11 led to better estimate fields but the dataset from additional two wells (BH04 and BH10) of these two data sets were reserved for validation purpose to be discussed later.

Field Experiments

With regard to the field experiments, the best-estimated T and S fields were selected using the same selection approach as in the synthetic aquifer but a different evaluation criterion since the field experiment did not have any known reference field. Specifically, they were determined according to the relative improvements in scatter plots and the evaluation criteria of the estimated $\ln T$ and $\ln S$ fields between the consecutive pairs of data sets of the previous-current, and current-following pumping wells (e.g., D#2 vs. D#3, and D#3 vs. D#4). That is, once there are no significant differences in the estimates using different data sets, the estimated fields are regarded as the best estimates. For example, we compared the

scatter plot of the estimated $\ln T$ using D#8 vs. those using D#9 (Figure 6a) and the scatter plot of the $\ln T$ estimates using D#9 vs. those using D#10 (Figure 6b). According to Figure 6a, the estimates using D#8 are closely correlated with those using D#9 as indicated by L1, L2, slope, and intercept of the regression line. On the other hand, the estimates using D#10 appears to be different from the estimates based on D#9 according to L1, L2, slope, and intercept of the regression line.

A comparison of the scatter plot of the estimated $\ln S$ of D#8 vs. that of D#9 (Figure 6c) and the scatter plot of the estimated from D#9 vs. the estimates from D#10 (Figure 6d) indicates that estimates from all the three data sets are similar.

The spatial distributions of T estimates for the three data sets are illustrated in Figure 7a, 7b, and 7c, while those of the corresponding S estimates are displayed in Figure 8a, 8b, and 8c. They all resemble each other. Based on these comparisons, we chose the estimated T and S fields (Figures 7b and 8b) using D#9 data sets as our best estimates for the field experiment. They will be used for the validation analysis.

Validation

Here, the validation means the assessment of the performance of the best-estimated T and S fields for predicting the evolution of drawdown fields induced by various pumping tests, which may or may not be used in the inversion process. This validation allows illustration and test of the previously defined completely redundant, moderately redundant, and highly nonredundant data set concept.

For the validation, the predictions used the same simulation domain, grids, initial and boundary conditions (46.44 m) discussed previously. Four cases were examined. Specifically, Case 1: Nine wells were used as either pumping or observation wells. Simulated heads at eight observation wells (excluding the pumping well) due to each pumping from the nine pumping wells were selected for the validation (see Table 2, D#9). Because all these 72

Table 2
Datasets of the Pumping Wells in the Inverse Modeling Using the HT in Both the Synthetic and Field Aquifers

Data Sets of Pumping Wells	Pumping Wells' Number	Total Data
D#2	BH06, 08	2
D#3	BH06, 08, 01	6
D#4	BH06, 08, 01, 07	12
D#5	BH06, 08, 01, 07, 09	20
D#6	BH06, 08, 01, 07, 09, 03	30
D#7	BH06, 08, 01, 07, 09, 03, 11	42
D#8	BH06, 08, 01, 07, 09, 03, 11, 02	56
D#9	BH06, 08, 01, 07, 09, 03, 11, 02, 05	72
D#10	BH06, 08, 01, 07, 09, 03, 11, 02, 05, 10	90
D#11	BH06, 08, 01, 07, 09, 03, 11, 02, 05, 10, 04	110

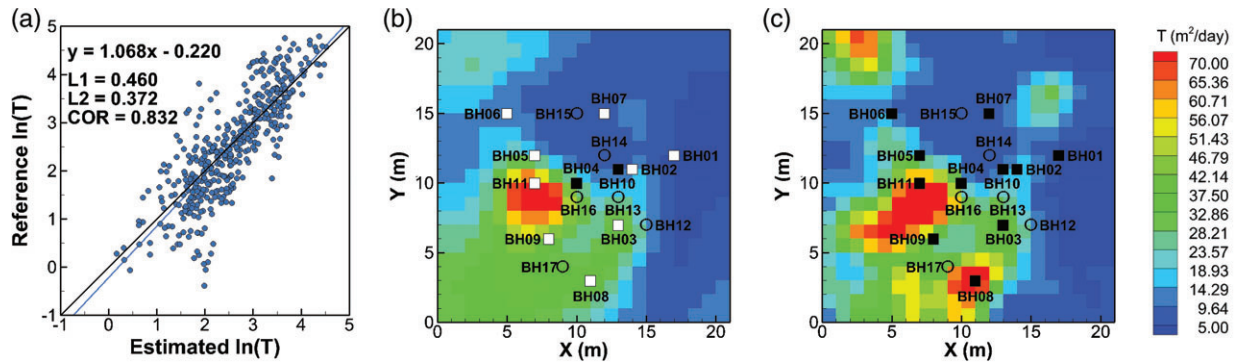


Figure 4. The best-estimated results based on the dataset of nine pumping wells (D#9) in the synthetic aquifer. (a) The scatter plots of the $\ln T$ field between the estimated and reference values, (b) the estimated T fields, and (c) the reference of T field. Nomenclature: the white squares denote the pumping well location. The open circles represent the six wells in 2" diameter are not used in the inverse modeling (note: each plot has 441 data sets).

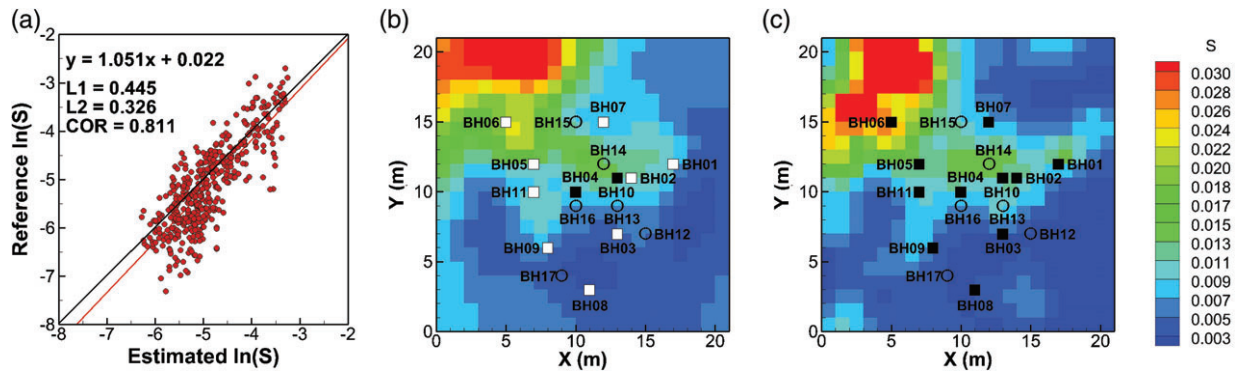


Figure 5. The best-estimated results based on the dataset of nine pumping wells (D#9) in the synthetic aquifer. (a) The scatter plots of the $\ln S$ field between the estimated and reference values, (b) the estimated S fields, and (c) the reference of S field. The nomenclature is the same as in Figure 4 (note: each plot has 441 datasets).

data sets were used in the HT inversion (or calibration), this case represents the result of the completely redundant data set.

Case 2: Heads at two wells (i.e., BH10 and BH04, not included in the nine wells) were simulated due to pumping from each of the nine pumping wells (as in case 1). This is the moderately redundant scenario since the two observation wells were not used in the calibration albeit the nine pumping wells were used before.

Case 3: Simulated heads at 10 observation wells (the nine wells plus either BH10 or BH04, depending which one was used as pumping well) during each pumping test at wells BH10 and BH04 were used for validation.

Case 4: BH10 and BH04 wells were pumped and the six wells in 2" diameter were used as observation wells. These 12 head data sets were used for the validation. As discussed previously, the six wells in 2" diameter and BH10 and BH04 were never used in inverse modeling. As a result, they are highly nonredundant data sets for testing the ability of the best-estimated T and S for prediction (see Table 3).

Synthetic Aquifer

The validation results for the synthetic aquifer are depicted in Figure 9a, 9b, 9c and 9d for cases 1, case 2,

case 3, and case 4, respectively. Figure 9a is the scatter plots of the result for case 1 using the nine pumping wells and eight observation wells (504 drawdown-time data) as those used in the inverse modeling. As expected, the data sets are completely redundant, and it is just a reproduction of the calibration result as evident by $L1 = 0.013$, $L2 = 0.001$, and $COR = 1.000$. That is, all the heterogeneity embedded in the 504 data is fully exploited in the best-estimated field. Although the simulated heads based on the true field closely agree with those predicted based on the best-estimated fields, the estimated fields are not the same as those of the reference fields as evident in Figures 4 and 5.

The scatter plot for case 2 (126 drawdown-time data), using the nine pumping wells and two observation wells, is displayed in Figure 9b. Since the pumping wells were used and the two observations (BH10 and BH04) were not used for deriving the best-estimated fields, the performance statistics of the validation are slightly worse (i.e., $L1 = 0.053$, $L2 = 0.008$, and $COR = 0.998$). As suggested by the cross-correlation analysis, the heterogeneity at the vicinity of the two observation wells is not well characterized in the best-estimated fields. This is likely the reason for the small scattering in the scatter plot.

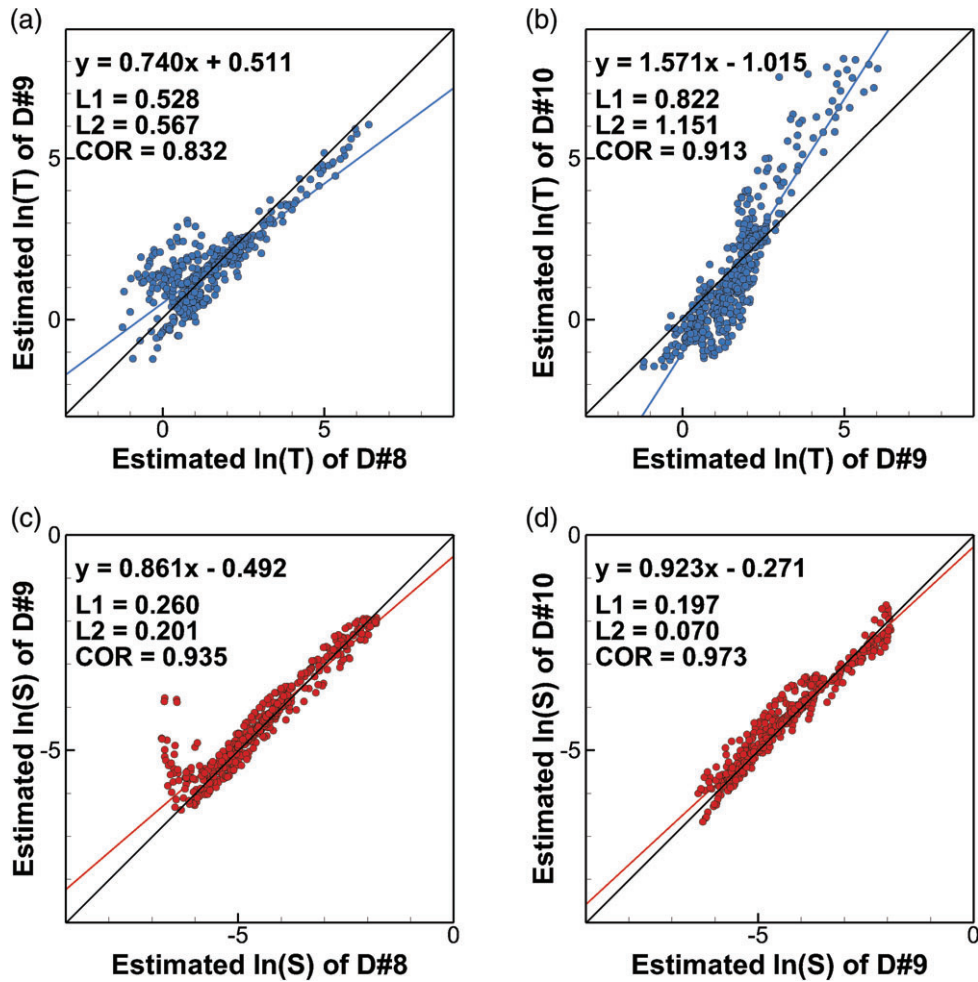


Figure 6. Comparison between the scatter plots of the $\ln T$ fields among the datasets of (a) D#8 vs. D#9, and (b) D#9 vs. D#10 in the field aquifer. The scatter plots of the $\ln S$ fields among the data sets of (c) D#8 vs. D#9, and (d) D#9 vs. D#10 in the field aquifer (note: each plot has 441 data sets).

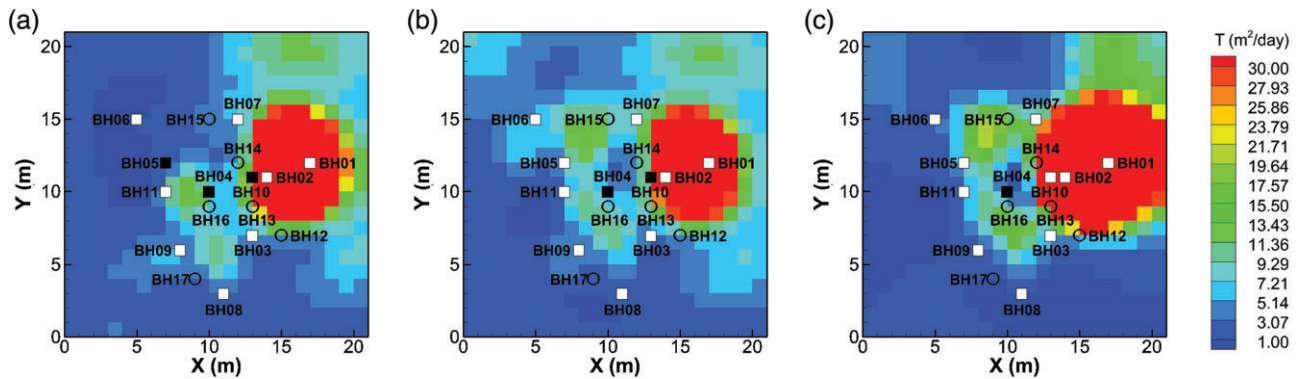


Figure 7. Comparison of the estimated T fields among the dataset of (a) D#8, (b) D#9, and (c) D#10 in the field aquifer. The nomenclature is the same as in Figure 4 (note: each plot has 441 data sets).

Similarly, Figure 9c shows the validation result for case 3 (140 drawdown-time data), in which 20 observation wells due to pumping test at two pumping wells (pumping at BH10 and BH04) were predicted and compared with those based on the reference field. The performance criteria are: $L1 = 0.062$, $L2 = 0.011$, and $COR = 0.998$, and they are slightly worse than those in case 1. Again,

the two pumping wells were not used in the HT inverse analysis to derive the best-estimated field; therefore, heterogeneity adjacent to the two wells was not fully resolved in the best-estimated field. In turn, the validation result is not as good as that in case 1. The result thus substantiates the moderate redundancy defined by the cross-correlation analysis.

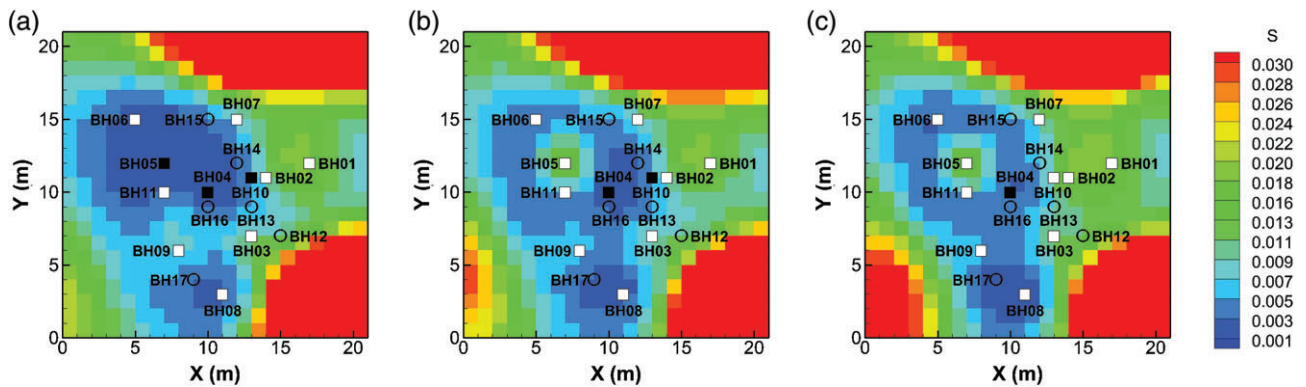


Figure 8. Comparison of the estimated S fields among the data set of (a) D#8, (b) D#9, and (c) D#10 in the field aquifer. The nomenclature is the same as in Figure 4 (note: each plot has 441 data sets).

Table 3
Definitions of Four Cases Using the Redundant/Nonredundant Information in Both the Synthetic and Field Aquifers (Note: Each Hydrograph Has Seven Sampling Points)

Cases	Types	Total Hydrography	Total Drawdown-Time Data
Case 1	Calibration: Using 9P (Pumping wells), each has 8O (Observation wells)	72	504
Case 2	Validation: Using 9P, each has 2O (i.e., BH10, BH04)	18	126
Case 3	Validation: Using 2P (i.e., BH10, BH04) \times 10O (9O + BH04 or BH10)	20	140
Case 4	Validation: Using 2P (BH10, BH04) \times (6O + [BH04 or BH10])	14	98

Finally, the highly nonredundant data sets case 4 is presented in Figure 9d. In this case, 98 drawdown-time data from the two pumping tests at BH10 and BH04 were simulated using the best-estimated T and S fields, and the simulated well hydrographs from the six observation wells in 2" diameter were selected to compare with those simulated heads in the true fields. Because these two pumping wells and the six wells in 2" diameter were never used in the HT analysis, this data set is called highly nonredundant, and the heterogeneity at the vicinity of these wells is likely not well resolved. As such, they have some effects on the predictions of the head behaviors at these locations as explained in the cross-correlation analysis. The resultant performance statistics ($L1 = 0.109$, $L2 = 0.025$, and $COR = 0.996$) support this reasoning as they are compared with those in cases 1, 2, and 3. Notice that no noise or uncertainty in the initial and boundary conditions are considered in these cases for the synthetic aquifers. The deterioration of validation is merely from the unresolved heterogeneity. That is to say, if data sets from BH10, BH04, and the six wells in 2" diameter are included in HT inverse analysis, the best-estimated fields using D#9 data sets would be improved.

Field Experiments

The scatter plots of the validation results for cases 1, 2, 3, and 4 of the field experiments are illustrated in Figure 10a, 10b, 10c, and 10d in the same style as those in Figure 9 for the synthetic aquifer. It should

be emphasized that in the field experiment case, the observed drawdown and measured pumping rates were likely subjected to errors as well as noise. In addition, the initial and boundary conditions used in the inverse modeling are our estimates, which were approximations of the true ones. Further, the flow in the field is always fully three-dimensional, while our inverse model is based on a two-dimensional depth-averaged model: model error exists. For these reasons, the scatter plot (Figure 10a) for case 1 (completely redundant data set) shows that predicted drawdown based on the best-estimated fields vs. the observed drawdown has larger dispersion than that in the synthetic case (Figure 9a) although overall it is unbiased as is the one in the synthetic aquifer.

Scatter plots for cases 2, 3, and 4 for the field aquifer exhibit a similar trend of deterioration of validation results as those in the synthetic aquifer. That is, the more nonredundant data sets are used in the validation, the scattering becomes more apparent. Once again, the field data corroborates the definitions of completely redundant, moderately redundant, and highly nonredundant data sets based on the cross-correlation analysis.

There are some differences in the validation results of cases 3 and 4 (where BH04 and BH10 were used as pumping wells) between the synthetic and field aquifers. In the synthetic aquifer, the heads in the nine wells due to pumping at BH04 (red circles in Figure 9c) or the heads due to pumping at BH10 (blue circles in Figure 9c)

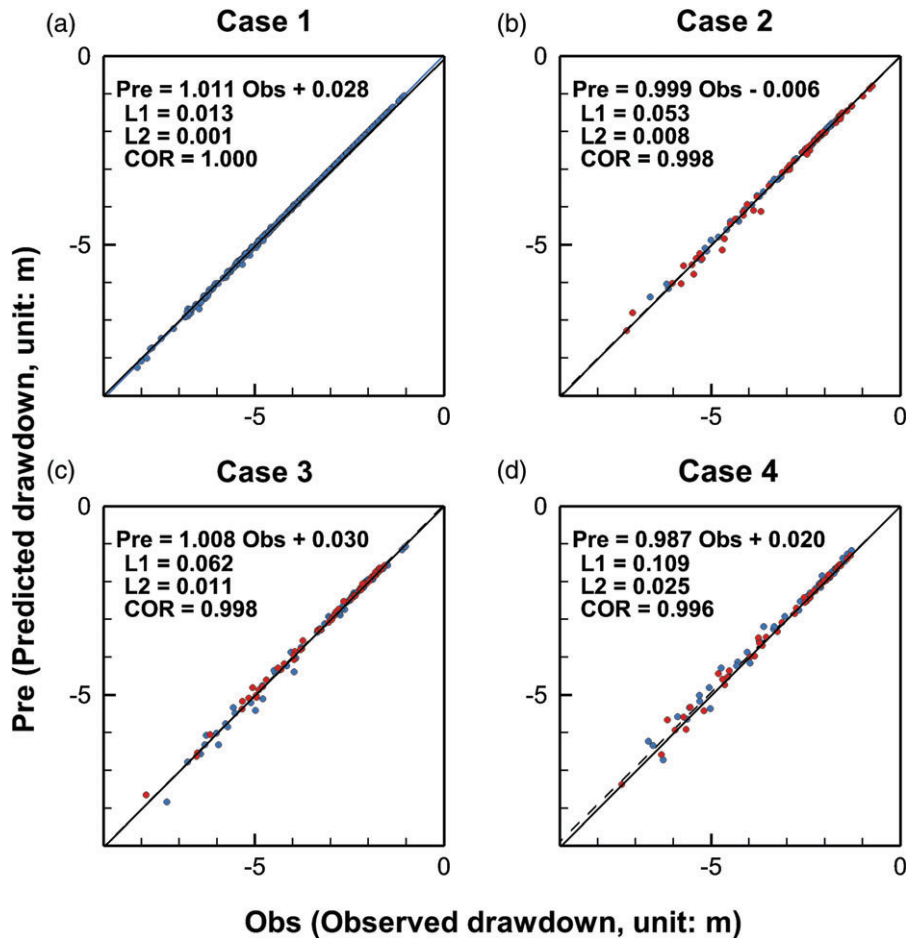


Figure 9. Scatter plots with logarithmic axes of the validation applying the best-estimated T and S fields using the HT from the synthetic aquifer to predict the drawdown-time data of pumping tests. (a) Case 1 (504 drawdown-time data), (b) case 2 (126 drawdown-time data), (c) case 3 (140 drawdown-time data), and (d) case 4 (98 drawdown-time data). (Note: the blue points of cases 3 and 4 denote pumping at BH10, the red points of cases 3 and 4 denote pumping at BH04.)

behave in a similar fashion as do the heads in the six wells in 2" diameter due to pumping at BH04 (red circles in Figure 9d) or due to pumping at BH10 (blue circles). Notice that BH04 and BH10, as well as the six wells in 2" diameter, were not used in the calibration.

To the contrary, in the field aquifer, the heads in either the nine wells or the six new wells, induced by pumping at BH04 well (red circles in Figures 10c and 10d), appear consistently scattering more than those triggered by pumping at BH10 well (blue circles in the figures). This anomalous behavior seems to suggest that BH04 and BH10 in the field aquifer are isolated from each other; BH04 is more connected to the nine wells and the new six wells than is BH10. This seems consistent with the best-estimated T and S fields in Figures 7b and 8b. This implies that inclusion of the nine well data induced by pumping at BH04 may significantly improve the validation using the six wells in 2" diameter.

Conclusions

This paper explores the completely/moderately redundant or highly nonredundant data sets for the HT

field campaign. Using the cross-correlation between heterogeneity anywhere of the aquifer and the observed heads at an observation well, induced by pumping at another well, the redundant and nonredundant concepts are defined. Subsequently, these definitions were tested and validated in a synthetic and a field aquifer involving sequential pumping tests, and the results are confirmative. Conclusions from the study are thus given below.

A completely redundant head dataset is defined as the head dataset that contains the same information about the heterogeneity distribution in the aquifer as does the one used earlier model calibration (or inverse modeling) effort. Such a data set will agree closely with the predicted heads based on the previously calibrated parameter fields. Because of this reason, the head data set will not yield improvements on the estimates from the earlier calibration.

On the other hand, the head data set contains partially new information about the heterogeneity of the aquifer is then called moderately nonredundant. A comparison of a moderately nonredundant head data set with the predicted heads from the previous calibration would reveal

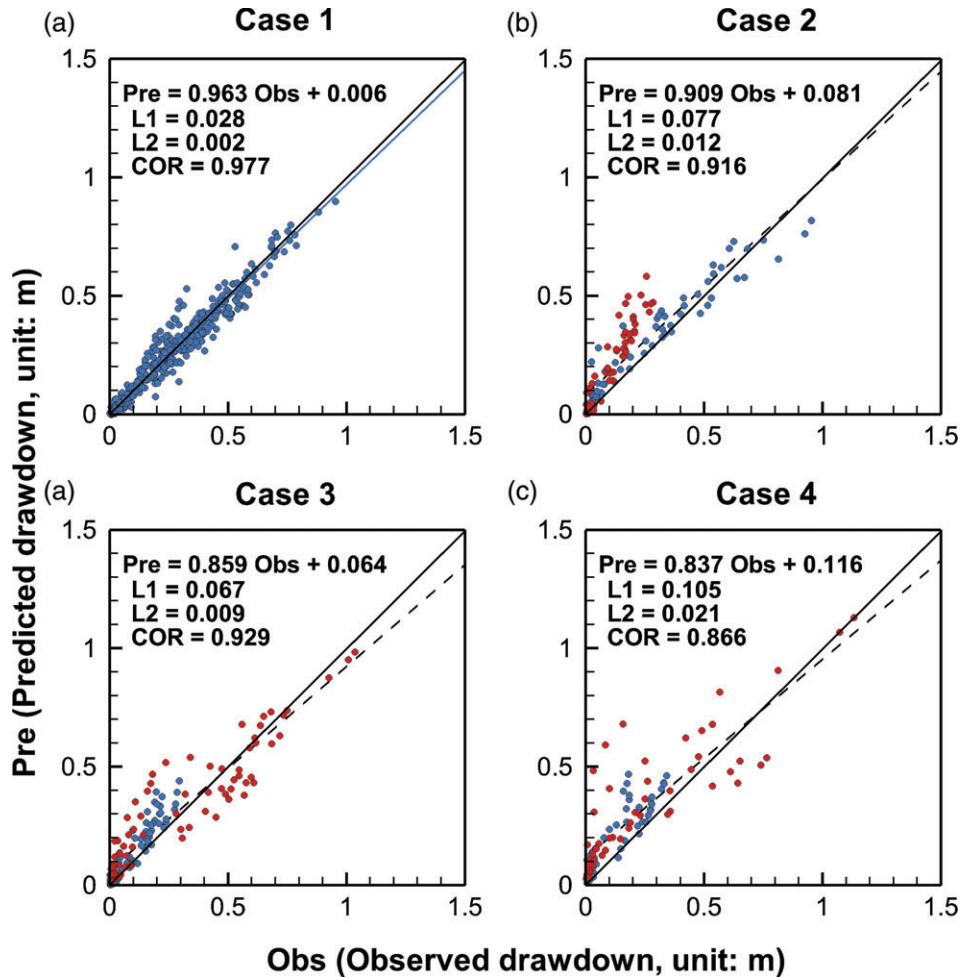


Figure 10. Scatter plots of the validation applying the best-estimated T and S fields using the HT from the field aquifer to predict the drawdown-time data of pumping tests. (a) Case 1 (504 drawdown-time data), (b) case 2 (126 drawdown-time data), (c) case 3 (140 drawdown-time data), and (d) case 4 (98 drawdown-time data). (Note: the blue points of cases 3 and 4 denote pumping at BH10, the red points of cases 3 and 4 denote pumping at BH04.)

small deviations. Such a moderately nonredundant dataset will further improve the estimates if it is included in model calibration. A potential example of such a data set is the head measurements at observation wells during a sequential pumping test but omitted in the previous calibration. Or the head measurements at existing wells induced by pumping at newly installed wells that are not used in previous model calibration efforts.

Lastly, data sets bring forth significantly new information about the heterogeneity distribution of the aquifer is defined as a highly nonredundant data set. Again, a comparison of this data set with the head predictions based on the previously calibration estimates would reveal larger deviations than the comparison of the moderately nonredundant data set. A potential example is the data set created from new pumping and observation well locations in the aquifer.

Overall, we believe the results of the study could help the design of hydraulic tomography tests to collect more information to enhance the characterizing of the aquifer and to correctly validate estimates from any inverse models.

Acknowledgments

Jet-Chau Wen would like to acknowledge the research support from NSC 101-2221-E-224-050, NSC 102-2221-E-224-050, MOST 103-2221-E-224-054, MOST 104-2221-E-224-039, MOST 104-2119-M-224-001, MOST 105-2625-M-224-002, MOST 106-2119-M-224-001, MOST 106-2625-M-224-002, MOST 106-2915-I-224-501, MOST 107-2119-M-224-001, MOST 107-2119-M-224-002, MOST 107-2625-M-224-002 and MOST 108-2625-M-224-002 by the Minister of Science and Technology, Taiwan. T.-C.J.Y. also acknowledges the support of the Global Expert award through Tianjin Normal University from the Thousand Talents Plan of Tianjin City. All data from this work are available upon request through the corresponding author.

Authors' Note

The authors do not have any conflicts of interest or financial disclosures to report.

References

- Berg, S.J., and W.A. Illman. 2011a. Capturing aquifer heterogeneity: Comparison of approaches through controlled sandbox experiments. *Water Resources Research* 47, no. 9: W09514. <https://doi.org/10.1029/2011WR010429>
- Berg, S.J., and W.A. Illman. 2011b. Three-dimensional transient hydraulic tomography in a highly heterogeneous glaciofluvial aquifer-aquard system. *Water Resources Research* 47, no. 10: W10507. <https://doi.org/10.1029/2011WR010616>
- Bohling, G., and J. Butler. 2010. Inherent limitations of hydraulic tomography. *Groundwater* 48, no. 6: 809–824. <https://doi.org/10.1111/j.1745-6584.2010.00757.x>
- Brauchler, R., R. Liedl, and P. Dietrich. 2003. A travel time based hydraulic tomographic approach. *Water Resources Research* 39, no. 12: 1370. <https://doi.org/10.1029/2003WR002262>
- Bruggeman, G.A. 1972. The reciprocity principle in flow through heterogeneous porous media. In *Fundamentals of Transport Phenomena in Porous Media*, 136–149. Amsterdam, The Netherlands: Elsevier.
- Cardiff, M., and W. Barrash. 2011. 3-D transient hydraulic tomography in unconfined aquifers with fast drainage response. *Water Resources Research* 47, no. 12: W12518. <https://doi.org/10.1029/2010WR010367>
- Castagna, M., and A. Bellin. 2009. A Bayesian approach for inversion of hydraulic tomographic data. *Water Resources Research* 45, no. 4: W04410. <https://doi.org/10.1029/2008WR007078>
- Chen, J.-L., J.-C. Wen, T.-C.J. Yeh, K.-Y.A. Lin, Y.-L. Wang, S.-Y. Huang, Y. Ma, C.-Y. Yu, and C.-H. Lee. 2019. Reproducibility of hydraulic tomography estimates and their predictions: A two-year case study in Taiwan. *Journal of Hydrology* 569: 117–134. <https://doi.org/10.1016/j.jhydrol.2018.11.064>
- Cooper, H.H. Jr., and C.E. Jacob. 1946. A generalized graphical method for evaluating formation constants and summarizing well-field history. *Eos, Transactions of the American Geophysical Union* 27, no. 4: 526–534.
- Fienen, M.N., T. Clemo, and P.K. Kitanidis. 2008. An interactive Bayesian geostatistical inverse protocol for hydraulic tomography. *Water Resources Research* 44, no. 12: W00B01. <https://doi.org/10.1029/2007WR006730>
- Gutjahr, A. L. 1989. Fast Fourier transforms for random field generation. In *Project Report for Los Alamos Grant*, Contract 4-R58-2690R, Socorro: Department of Mathematics, N. M. Tech.
- Hao, Y., T.-C.J. Yeh, W.A. Illman, K. Ando, and K.-C. Hsu. 2008. Hydraulic tomography for detecting fracture zone connectivity. *Groundwater* 46, no. 2: 183–192. <https://doi.org/10.1111/j.1745-6584.2007.00388.x>
- Huang, S.-Y., J.-C. Wen, T.-C.J. Yeh, W. Lu, H.-L. Juan, C.-M. Tseng, J.-H. Lee, and K.-C. Chang. 2011. Robustness of joint interpretation of sequential pumping tests: Numerical and field experiments. *Water Resources Research* 47, no. 10: W10530. <https://doi.org/10.1029/2011WR010698>
- Illman, W.A., X. Liu, and A. Craig. 2007. Steady-state hydraulic tomography in a laboratory aquifer with deterministic heterogeneity: Multimethod and multiscale validation of K tomograms. *Journal of Hydrology* 341, no. 3–4: 222–234. <https://doi.org/10.1016/j.jhydrol.2007.05.011>
- Illman, W.A., X. Liu, and A.J. Craig. 2008. Evaluation of transient hydraulic tomography and common hydraulic characterization approaches through laboratory sandbox experiments. *Environmental Engineering and Management Journal* 18, no. 4: 249–256.
- Illman, W.A., X. Liu, S. Takeuchi, T.-C.J. Yeh, K. Ando, and H. Saegusa. 2009. Hydraulic tomography in fractured granite: Mizunami underground research site, Japan. *Water Resources Research* 45, no. 1: W01406. <https://doi.org/10.1029/2007WR006715>
- Illman, W.A., S.J. Berg, X. Liu, and A. Massi. 2010. Hydraulic/partitioning tracer tomography for DNAPL source zone characterization: Small-scale sandbox experiments. *Environmental Science and Technology* 44, no. 22: 8609–8614. <https://doi.org/10.1021/es101654j>
- Illman, W.A., S.J. Berg, and T.-C.J. Yeh. 2012. Comparison of approaches for predicting solute transport: Sandbox experiments. *Groundwater* 50, no. 3: 421–431. <https://doi.org/10.1111/j.1745-6584.2011.00859.x>
- Illman, W.A., S.J. Berg, and Z. Zhao. 2015. Should hydraulic tomography data be interpreted using geostatistical inverse modeling? A laboratory sandbox investigation. *Water Resources Research* 51, no. 5: 3219–3237. <https://doi.org/10.1002/2014WR016552>
- Li, W., W. Nowak, and O.A. Cirpka. 2005. Geostatistical inverse modeling of transient pumping tests using temporal moments of drawdown. *Water Resources Research* 41, no. 8: W08403. <https://doi.org/10.1029/2004WR003874>
- Liu, X., and P.K. Kitanidis. 2011. Large-scale inverse modeling with an application in hydraulic tomography. *Water Resources Research* 47, no. 2: W02501. <https://doi.org/10.1029/2010WR009144>
- Liu, S., T.-C.J. Yeh, and R. Gardiner. 2002. Effectiveness of hydraulic tomography: Sandbox experiments. *Water Resources Research* 38, no. 4: 1034. <https://doi.org/10.1029/2001WR000338>
- Liu, X., W.A. Illman, A.J. Craig, J. Zhu, and T.-C.J. Yeh. 2007. Laboratory sandbox validation of transient hydraulic tomography. *Water Resources Research* 43, no. 5: W05404. <https://doi.org/10.1029/2006WR005144>
- Mao, D., L. Wan, T.-C.J. Yeh, C.-H. Lee, K.-C. Hsu, J.-C. Wen, and W. Lu. 2011. A revisit of drawdown behavior during pumping in unconfined aquifers. *Water Resources Research* 47, no. 5: W05502. <https://doi.org/10.1029/2012WR009326>
- Mao, D., T.-C.J. Yeh, L. Wan, C.-H. Lee, K.-C. Hsu, J.-C. Wen, and W. Lu. 2013a. Cross-correlation analysis and information content of observed heads during pumping in unconfined aquifers. *Water Resources Research* 49, no. 2: 713–731. <https://doi.org/10.1002/wrcr.20066>
- Mao, D., T.-C.J. Yeh, L. Wan, K.-C. Hsu, C.-H. Lee, and J.-C. Wen. 2013b. Necessary conditions for inverse modeling of flow through variably saturated porous media. *Advances in Water Resources* 52: 50–61. <https://doi.org/10.1016/j.advwatres.2012.08.001>
- Mao, D., T.-C.J. Yeh, L. Wan, J.-C. Wen, W. Lu, C.-H. Lee, and K.-C. Hsu. 2013c. Joint interpretation of sequential pumping tests in unconfined aquifers. *Water Resources Research* 49, no. 4: 1782–1796. <https://doi.org/10.1002/wrcr.20129>
- Ni, C.-F., and T.-C.J. Yeh. 2008. Stochastic inversion of pneumatic cross-hole tests and barometric pressure fluctuations in heterogeneous unsaturated formations. *Advances in Water Resources* 31, no. 12: 1708–1718. <https://doi.org/10.1016/j.advwatres.2008.08.007>
- Ni, C.-F., T.-C.J. Yeh, and J.-S. Chen. 2009. Cost-effective hydraulic tomography surveys for predicting flow and transport in heterogeneous aquifers. *Environmental Science and Technology* 43, no. 10: 3720–3727. <https://doi.org/10.1021/es8024098>
- Robin, M.J.L., A.L. Gutjahr, E.A. Sudicky, and J.L. Wilson. 1993. Cross-correlated random field generation with the direct Fourier transform method. *Water Resources Research* 29, no. 7: 2385–2397. <https://doi.org/10.1029/93WR00386>
- Sun, R., T.-C.J. Yeh, D. Mao, M. Jin, W. Lu, and Y. Hao. 2013. A temporal sampling strategy for hydraulic tomography analysis. *Water Resources Research* 49, no. 7: 3881–3896. <https://doi.org/10.1002/wrcr.20337>
- Theis, C.V. 1935. The relation between lowering the piezometric surface and the rate and duration of discharge of a well using ground water storage. *Eos, Transactions of the American Geophysical Union* 16, no. 12:519–524.

- Tso, C.-H.M., Y. Zha, T.-C.J. Yeh, and J.-C. Wen. 2016. The relative importance of head, flux, and prior information in hydraulic tomography analysis. *Water Resources Research* 52, no. 1: 3–20. <https://doi.org/10.1002/2015WR017191>
- Wen, J.-C., C.-M. Wu, T.-C.J. Yeh, and C.-M. Tseng. 2010. Estimation of effective aquifer hydraulic properties from an aquifer test with multi-well observations (Taiwan). *Hydrogeology Journal* 18, no. 5: 1143–1155. <https://doi.org/10.1007/s10040-010-0577-1>
- Wu, C.-M., T.-C.J. Yeh, J. Zhu, T.H. Lee, N.-S. Hsu, C.-H. Chen, and A.F. Sancho. 2005. Traditional analysis of aquifer tests: Comparing apples to oranges? *Water Resources Research* 41, no. 9: W09402. <https://doi.org/10.1029/2004WR003717>
- Xiang, J., T.-C.J. Yeh, C.-H. Lee, K.-C. Hsu, and J.-C. Wen. 2009. A simultaneous successive linear estimator and a guide for hydraulic tomography analysis. *Water Resources Research* 45, no. 2: W02432. <https://doi.org/10.1029/2008WR007180>
- Yeh, T.-C.J., and S. Liu. 2000. Hydraulic tomography: Development of a new aquifer test method. *Water Resources Research* 36, no. 8: 2095–2105. <https://doi.org/10.1029/2000WR900114>
- Yeh, T.-C.J., R. Srivastava, A. Guzman, and T. Harter. 1993. A numerical model for water flow and chemical transport in variably saturated porous media. *Groundwater* 31, no. 4: 634–644. <https://doi.org/10.1111/j.1745-6584.1993.tb00597.x>
- Yeh, T.-C.J., D. Mao, Y. Zha, J.-C. Wen, L. Wan, K.-C. Hsu, and C.-H. Lee. 2015. Uniqueness, scale, and resolution issues in groundwater model parameter identification. *Water Science and Engineering* 8, no. 3: 175–194. <https://doi.org/10.1016/j.wse.2015.08.002>
- Yin, D., and W.A. Illman. 2009. Hydraulic tomography using temporal moments of drawdown recovery data: A laboratory sandbox study. *Water Resources Research* 45, no. 1: W01502. <https://doi.org/10.1029/2007WR006623>
- Zha, Y., T.-C.J. Yeh, W.A. Illman, T. Tanaka, P. Bruines, H. Onoe, and H. Saegusa. 2015. What does hydraulic tomography tell us about fractured geological media? A field study and synthetic experiments. *Journal of Hydrology* 531: 17–30. <https://doi.org/10.1016/j.jhydrol.2015.06.013>
- Zha, Y., T.-C.J. Yeh, W.A. Illman, T. Tanaka, P. Bruines, H. Onoe, H. Saegusa, D. Mao, S. Takeuchi, and J.-C. Wen. 2016. An application of hydraulic tomography to a large-scale fractured granite site, Mizunami, Japan. *Groundwater* 54, no. 6: 793–804. <https://doi.org/10.1111/gwat.12421>
- Zhao, Z., and W.A. Illman. 2017. On the importance of geological data for three-dimensional steady state hydraulic tomography at a highly heterogeneous aquifer-aquitard system. *Journal of Hydrology* 544: 640–657. <https://doi.org/10.1016/j.jhydrol.2016.12.004>
- Zhao, Z., and W.A. Illman. 2018. Three-dimensional imaging of aquifer and aquitard heterogeneity via transient hydraulic tomography at a highly heterogeneous field site. *Journal of Hydrology* 559: 392–410. <https://doi.org/10.1016/j.jhydrol.2018.02.024>
- Zhao, Z.F., W.A. Illman, T.-C.J. Yeh, S.J. Berg, and D. Mao. 2015. Validation of hydraulic tomography in an unconfined aquifer: A controlled sandbox study. *Water Resources Research* 51, no. 6: 4137–4155. <https://doi.org/10.1002/2015wr016910>
- Zhao, Z., W.A. Illman, and S.J. Berg. 2016. On the importance of geological data for hydraulic tomography analysis: Laboratory sandbox study. *Journal of Hydrology* 542: 156–171. <https://doi.org/10.1016/j.jhydrol.2016.08.061>
- Zhu, J., and T.-C.J. Yeh. 2005. Characterization of aquifer heterogeneity using transient hydraulic tomography. *Water Resources Research* 41, no. 7: W07028. <https://doi.org/10.1029/2010WR003790>
- Zhu, J., and T.-C.J. Yeh. 2006. Analysis of hydraulic tomography using temporal moments of drawdown recovery data. *Water Resources Research* 42, no. 2: W02403. <https://doi.org/10.1029/2005WR004309>